THE SOCIETY OF NAVAL ARCHITECTS AND MARINE ENGINEERS
601 Pavonia Avenue, Jersey City, NJ 07306
Paper to be presented at the Propellers '88 Symposium,
Virginia Beach, Virginia, September 20-21, 1988

# On the Optimum Ducted Propeller Loading No. 1

**S. A. Kinnas,** Associate Member and **W.B. Coney,** Student Member, Massachusetts Institute of Technology, Cambridge, MA

## Abstract

A numerical approach to determine the optimum circulation distibution of a propeller inside a given duct is presented. The propeller blades are modelled by lifting lines. The duct is represented in non-linear theory by using a potential based panel method.

The propeller lifting lines are approximated by a finite number of vortex horseshoes. The strengths of the horseshoes are determined by using a numerical non-linear optimization technique to maximize the propulsor efficiency. The non-axisymmetric duct/propeller interactions are included within the design procedure.

Results are presented for propellers designed to operate at various thrust coefficients inside of two different ducts and at several advance ratios.

## 1 Introduction

Ducted propellers have been an alternative form of propulsion during the last sixty years with aplications ranging from supertankers to remote operating vehicles and fishing vessels. Their purpose has been either to increase efficiency or to reduce the cavitation of the propulsor as well as to protect the propeller from damage.

The analysis of the flow around a ducted propeller has evolved together with the evolution of numerical methods for the analysis of the flow around propellers and ducts.

The first generation of analysis methods represented the duct in linear theory by distributing ring vortices and sources on a approximate mean surface. The propeller was represented by using actuator disc, lifting line or lifting surface theories. Some representative works in that area have been published by Morgan[11], Caster[3] and Dyne[6].

The next generation of analysis methods represented the duct in non-linear theory by distributing surface vorticity on the duct, and represented the propeller with actuator disc or lifting line theory. Ryan and Glover[17], Gibson and Lewis[7] and Falcão de Campos[4] are some of the investigators who have made contributions in that area.

All of the previous methods however, have assumed that the interactions between the duct and the propeller were axisymmetric.

It is only recently that the non-axisymmetric flow in a ducted propeller has been adressed by solving for the flow around the duct induced by the non-axisymmetric flow field due to the propeller. VanHouten[15] and Feng and Dong[5] have published works in that area.

Very recently, Kerwin, Kinnas et al.[9] have developed a method for the analysis of ducted propellers in which the flow on the duct is analyzed by using a potential based panel method and the flow on the propeller is analyzed by using a lifting surface method. In that work a strong angular variation of the circulation around a duct, and of the pressure distributions on the surface of a duct working with a propeller, has been presented. They conclude that the circumferential variation of the duct-propeller interaction is important and should be included in the analysis of the flow of a ducted propeller.

The design of ducted propellers until recently, has been achieved by a "trial and error" procedure. In detail, for specified advance coefficient, thrust coefficient and duct thrust/propeller thrust ratio, a preliminary design is determined. That design is then consequetively modified and verified by using any of the previously cited analysis methods, until the design objectives are met.

The preliminary ducted propeller loading has been selected to minimize the absorbed power for a given thrust of the propulsor. The optimum ducted propeller loading has usually been determined from momentum theory. This procedure, however, does not allow for finite number of blades and for detailed duct geometry. Sparenberg [18] and [19] determined the optimum ducted propeller loading by representing the propeller with lifting lines and the duct with a concentrated ring vortex of varying strength circumferentially.

In the present work a new approach is developed in order to determine the optimum circulation distribution of a propeller operating inside a given duct. The propeller is replaced with lifting lines, which are then approximated by a finite number of vortex horseshoes.

The duct is represented in non-linear theory by using a potential based panel method. The strengths of the lifting line horseshoes, and thus the propeller loading, are then determined such as to maximize the propulsive device efficiency by using a numerical non-linear optimization technique.

The advantages of the presented design approach are threefold.

- It offers a systematic mathematical way to determine the optimum ducted propeller loading.
- The duct is represented in non-linear theory within the design procedure.
- The non-axisymmetric duct-propeller interactions are considered within the design process.

## 2 Analysis of the Flow Around the Duct

The geometry of the duct as shown in Figure 1 is defined by the following parameters:

- The chordlength, c, which is defined as the nose-tail distance of the duct section.
- The radius, $R_{in}$, at the nose of the duct.
- The angle, $\alpha$, of the duct section with respect to the axis of the duct.
- The section of the duct, defined as the cut of the duct with the meridional planes.
- The camber distribution, $f(x)$, and thickness distribution, $t(x)$, of the duct section, defined in the same way as for a hydrofoil section. Positive camber points inside the duct.

The ducts to be considered in this paper are axisymmetric. A brief discussion about the treatment of non-axisymmetric ducts can be found in Section 7.

The flow around the duct is assumed to be inviscid, incompressible and irrotational. If the incoming velocity field is given by $\vec{U}_{in}$, then the velocity flowfield, $\vec{q}$, around the duct can be expressed in terms of the perturbation velocity potential, $\phi$, defined as follows:

$$\vec{q} = \vec{U}_{in} + \nabla\phi. \tag{1}$$

The analysis of the flow around a duct in uniform flow, as well as the analysis of a duct working with a given propeller has recently been treated by using a potential based panel method as described by Kerwin, Kinnas et al. [9].

In this paper the propeller will be modelled by radial lifting lines. Therefore, we will concentrate on solving the problem of a duct with lifting lines of given strength and with given pitch at their trailing wakes. The projected geometry of one lifting line on the duct meridional plane can be seen in Figure 2. The lifting line is located at $x = x_{LL}$ and the corresponding propeller radius is defined equal to the radius of the duct at $x_{LL}$, as shown in Figure 2.

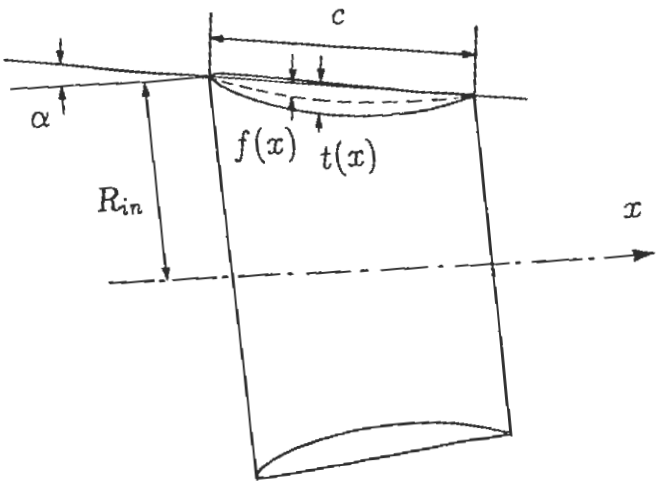


Figure 1: Geometry of the Duct

The perturbation potential, $\phi_D$, on the duct can be found by applying Green's theorem on the duct surface:

$$\begin{aligned} 2\pi\phi_D(P) = & \iint_{S_D} \left[\phi_D(Q)\frac{\partial}{\partial n_Q}\frac{1}{R(P;Q)} \right. \\ & \left. - \frac{\partial\phi_D(Q)}{\partial n_Q}\frac{1}{R(P;Q)}\right] dS \\ & + \iint_{S_W} \Delta\phi_D(Q)\frac{\partial}{\partial n_Q}\frac{1}{R(P;Q)} dS \\ & + 4\pi \quad \phi_{LL}(P). \end{aligned} \tag{2}$$

- $P$ corresponds to any point on the duct surface $S_D$.
- $Q$ corresponds to any point on $S_D$ and the duct wake surface $S_W$.
- $R(P;Q)$ is the distance between the points $P$ and $Q$ and actually corresponds to the infinite fluid domain Green's function.
- $\phi_{LL}$ is the potential on the duct due to the propeller lifting lines.
- $\Delta\phi_D$ is the jump of the potential in the wake of the duct.

Equation 2 is a Fredholm integral equation of the second kind with respect to the unknown potential $\phi_D$. It expresses the potential $\phi_D$ in terms of source and dipole distributions on the duct and wake surfaces. The strength of the sources is given by the kinematic boundary condition:

$$\frac{\partial\phi_D}{\partial n_Q} = -\vec{U}_{in}\cdot\vec{n}_Q. \tag{3}$$

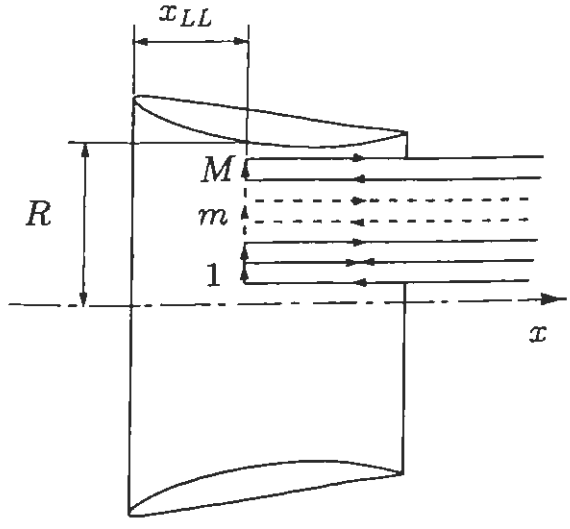


Figure 2: Duct with lifting line.

The incoming velocity with respect to the rotating lifting lines frame, $\vec{U}_{in}$ is given as:

$$\vec{U}_{in} = \vec{U}_\infty + \vec{\omega} \times \vec{r}. \tag{4}$$

- $\vec{U}_\infty$ is the freestream velocity, $V_S$, for a duct operating in open water.
- $\vec{\omega}$ is the angular velocity of the lifting lines.
- $\vec{r}$ is the radial distance of the point from the axis of the duct.

The solution to equation 2 is achieved numerically by approximating the duct surface and its trailing wake with quadrilateral panels as shown in Figure 3. The dipole and source distributions on the panels are approximated by constant strength distributions. The stength of the sources is known and given by 3. The strength of the dipoles in the wake is set equal to the difference of the potentials at the upper and lower panels at the trailing edge of the duct as suggested by Morino [12]. The discretized equation 2 is then applied at some appropriately selected control points, and the resulting system of linear equations is inverted with respect to the unknown dipole strengths, i.e. the potentials. More details about the numerical method can be found in Kerwin, Kinnas et al. [9].

The surface velocities on the duct are determined by differentiating the potential with respect to the curvilinear directions on the duct. The pressures on the duct are then determined by applying Bernoulli's equation:

$$p_\infty + \frac{\rho}{2}U_\infty^2 = p + \frac{\rho}{2}q^2 - \frac{1}{2}(\vec{\omega} \times \vec{r})^2. \tag{5}$$

where:

- $p$ is the pressure at a given point.
- $q$ is the magnitude of the flowfield velocity with respect to a frame rotating with the lifting lines.
- $p_\infty$ is the pressure of the undisturbed flow.
- $\rho$ is the density of the fluid.

The pressure coefficient, $C_p$, is defined as:

$$C_p = \frac{p - p_\infty}{\frac{\rho}{2}U_\infty^2} \tag{6}$$

The forces on the duct are found by summing the individual vector forces on each panel. We have found this procedure to be adequate in predicting the forces, and in particular the duct thrust, with satisfactory accuracy.

The pressure distributions on the duct, resulting from a panel calculation, are shown in Figure 4. The substantial non-axisymmetry of the flow field around the duct is evident from Figure 4. One of the objectives of this paper is to include this non-axisymmetry within the design procedure of a ducted propeller.

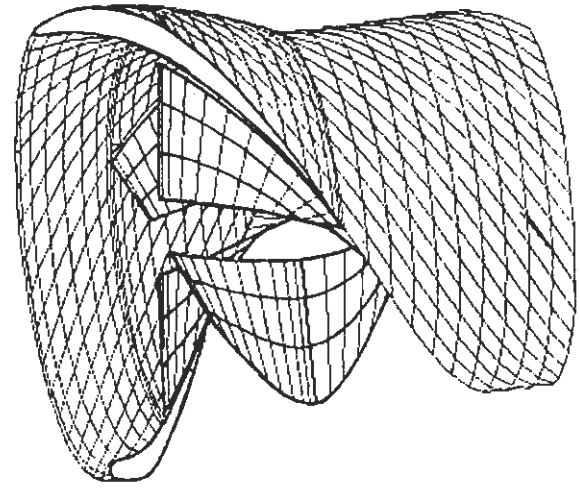

Figure 3: Panel arrangement on the duct and the lifting lines. For this drawing 40 chordwise and 40 circumferential panels have been used to panel the duct with only half of them shown. The four equally spaced lifting lines are broken into three horsehoes of equal span. The wake of the duct is also panelled, but only a part of it, extending one duct chordlength downstream, is shown. The panelling on the duct and its wake is aligned with the panelling of the horseshoes at the tip of the lifting lines.

The issue of the flow in the gap between the propeller tip and the duct has been briefly addressed by Kerwin, Kinnas, et al. They concluded that the results from the analysis of the potential flow around a ducted propeller, are physically meaningful in the case of zero gap or large gap relative to the propeller radius. The results for intermediate gaps, for example one percent of the propeller radius, are expected to be unrealistic, since for those gaps the cross flow between the trailing tip vortex and the duct is dominated by viscous effects. A possible way to model the cross flow at the gap, via the "orifice equation", was suggested by Kerwin, Kinnas et al. [9]. However, the application of that technique will be left for future papers. Therefore, we will finally consider only lifting lines with zero gaps, since this is the only feasible case, in the context of potential theory, which is of practical interest.

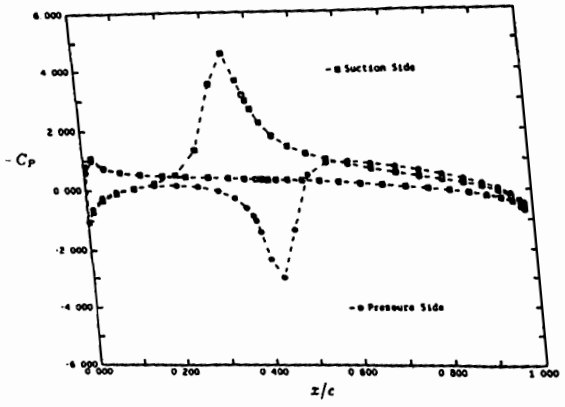


Figure 4: This is a plot of the pressure coefficient $C_p = 2(p - p_\infty)/(\rho U_\infty^2)$ vs chordwise location for lifting lines inside a duct with zero tip gap. The pressure distributions are shown around two duct strips, one close to the suction side of the lifting lines and the other close to the pressure side. This calculation has been done by using 60 chordwise and 60 circumferential panels on the duct. The pitch angle of the four lifting lines is equal to 30 degrees. The strength of the lifting lines is constant along the span and given by $\frac{\Gamma}{2\pi R U_\infty} = 0.1$.

# 3 The Optimum Propeller Load Distribution

## 3.1 The Propeller Lifting Line Model

A vortex lattice system of lifting lines is used to represent the propeller. The fundamental assumptions of this lifting line model are:

- the propeller blades are represented by straight, radial lifting lines;
- the blades are considered to have equal angular spacing and identical loading;
- the wake geometry is assumed to be purely helical, with a pitch at each radius determined by the undisturbed inflow (linear theory) or by the induced flow at the lifting line (moderately loaded theory).

The continuous distribution of bound vorticity along the lifting line is discretized by a vortex lattice of straight line elements of constant strength and of equal length. At the ends of each of these vortex segments a helical trailing vortex is shed into the wake. Each bound vortex segment and its two accompanying helical vortices is referred to as a "horseshoe" vortex. The velocities induced on the control points (located at the center of each of the bound vortex segments) by this system of vorticity can be found by the very efficient asymptotic formulas developed by Wrench [20].

The force acting at a radius $r$ on the lifting line is derived from a local application of Kutta-Joukowski's law. The axial and tangential induced velocities combine with the inflow and rotational velocity to produce an effective inflow of magnitude $V^*(r)$ directed at an angle $\beta_i(r)$ with respect to the plane of rotation. A force per unit radius

$$F(r) = \rho V^*(r)\Gamma(r)$$

is directed at right angles to $V^*(r)$ as shown in Figure 5. The effect of viscous drag is included by adding a force $F_v(r)$ acting in a direction parallel to $V^*$. This force is estimated on the basis of an experimentally determined two-dimensionsal sectional drag coefficient, $C_D(r)$. This means, of course, that the section chord lengths $c(r)$, must be specified.

The resultant force may then be resolved into axial and tangential components.

$$\begin{aligned} F_x(r) &= \rho V^*(r)\Gamma(r)\cos\beta_i(r) \\ &\quad - \frac{1}{2}\rho|V^*(r)|^2 c(r) C_D(r)\sin\beta_i(r), \\ F_t(r) &= \rho V^*(r)\Gamma(r)\sin\beta_i(r) \\ &\quad + \frac{1}{2}\rho|V^*(r)|^2 c(r) C_D(r)\cos\beta_i(r). \end{aligned} \tag{7}$$

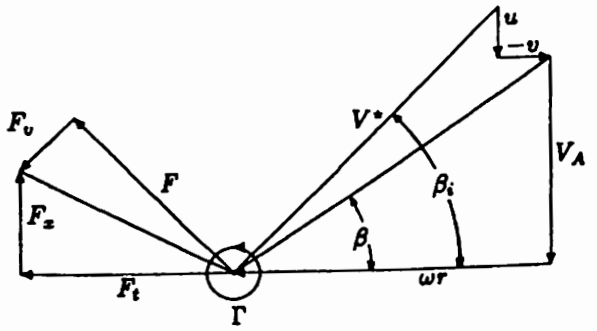


Figure 5: Velocity and Force diagram for a lifting line.

Under the discrete model used in the present theory the total forces on the propeller become:

$$\begin{aligned} T &= \rho K \sum_{m=1}^{M} \Big( V_m^* \Gamma_m \cos\beta_{im} \\ &\quad - \frac{1}{2} V_m^{*2} c_m C_{Dm} \sin\beta_{im} \Big) \Delta r, \\ Q &= \rho K \sum_{m=1}^{M} \Big( V_m^* \Gamma_m \sin\beta_{im} \\ &\quad + \frac{1}{2} V_m^{*2} c_m C_{Dm} \cos\beta_{im} \Big) r_m \Delta r; \end{aligned} \quad (8)$$

where $K$ is the number of blades, $M$ is the number of control points and $\Delta r$ is the length of a vortex segment.

## 3.2 The Variational Circulation Optimization Procedure

This is the classical problem of finding the optimum radial distribution of circulation given a propeller's operating conditions. Our goal is to find the circulation distribution which provides a prescribed thrust, $T$, for a minimum torque, $Q$. We begin with an inviscid vortex lattice model with a frozen wake geometry. The thrust and torque are given by:

$$\begin{aligned} T &= \rho K \sum_{m=1}^{M} (V_{Tm} + \omega r_m + v_m) \Gamma_m \Delta r_m, \\ Q &= \rho K \sum_{m=1}^{M} (V_{Am} + u_m) \Gamma_m r_m \Delta r_m; \end{aligned} \quad (9)$$

where

$$\begin{aligned} u_m &= \sum_{n=1}^{M} \Gamma_n u^*_{m,n}, \\ v_m &= \sum_{n=1}^{M} \Gamma_n v^*_{m,n}. \end{aligned} \quad (10)$$

$\Delta r_m$ is the radial distance between the two lattice points surrounding control point $m$, and $u^*_{m,n}$, $v^*_{m,n}$ are the velocities induced on control point $m$ by unit circulation on the horseshoe vortex surrounding control point $n$.

Using a variational approach, we form the quantity $H = Q + \lambda T$ which is to be minimized. The Lagrange multiplier, $\lambda$, is to be solved for along with the $\Gamma_m$'s. Expanding $H$ with equations 9 and 10 and then setting its partial derivatives with respect to the $\Gamma_m$'s equal to zero, gives us $M$ equations for the $M$ discrete values of circulation and the Lagrange multiplier. An additional equation is provided by specifying the required thrust in equation 9.

$$\begin{aligned} \frac{\partial H}{\partial \Gamma_i} = 0 &= \rho K \{ V_{Ai} r_i \Delta r_i \\ &\quad + \sum_{m=1}^{M} (\Gamma_m u^*_{i,m} r_m \Delta r_m + \Gamma_m u^*_{m,i} r_i \Delta r_i) \\ &\quad + \lambda (V_{Ti} + \omega r_i) \Delta r_i \\ &\quad + \tilde{\lambda} \sum_{m=1}^{M} (\Gamma_m v^*_{i,m} \Delta r_m + \Gamma_m v^*_{m,i} \Delta r_i) \}, \\ &\quad (i = 1, \ldots, M); \\ T &= \rho K \sum_{m=1}^{M} (V_{Tm} + \omega r_m + v_m) \Gamma_m \Delta r_m. \end{aligned} \quad (11)$$

The constants, $\tilde{\lambda}$ and the $v_m$'s, in the thrust equation are determined by equations 11 and 10 during a previous iteration of these optimization equations. This iterative approach allows us to include a simple model for viscosity. The effect of viscous drag on the total thrust can be included by adding a drag computed during the previous iteration to the thrust required in the current iteration. The effect of viscous drag on the optimum circulation distribution is currently ignored.

## 3.3 Chord Length Selection

The radial distribution of chord length is a necessary input to the viscous force calculations of the variational circulation optimization. The chord lengths are usually selected through cavitation considerations. Since the local cavitation number is a function of the induced velocity, which in turn depends on the circulation distribution, it may be desirable to select the chord lengths as part of the circulation optimization procedure. If this is done the chord lengths are updated after each iteration of the variational circulation optimization. The chord length selection process described here requires the input of the local cavitation number and circulation at each control point, as well as the blade thickness and a minimum chord length at the hub. The thickness distribution and the hub chord are input based on strength of materials considerations.

The chord shape is defined by a third order b-spline, as described by Rogers and Adams [16], with either four or five vertices. The vertices are chosen so that the resulting chord lengths vary smoothly from the input hub chord length. The chord lengths are required to be everywhere greater than the minimum chord lengths from the cavitation considerations described below. The use of b-splines insures a smooth curve defined by only a few points.

The foil section is assumed to be a NACA 66 (TMB modified nose and tail) profile with a NACA $a = 0.8$ meanline. Brockett [2] presents a figure showing the optimum geometry for a given minimum pressure coefficient for this section. Kroeger [10] mapped this figure to the following equation:

$$\sigma(r) = 26.67\left(\frac{f(r)}{c(r)}\right)^2 + 8.09\left(\frac{f(r)}{c(r)}\right) + 10.0\left(\frac{f(r)t(r)}{c(r)c(r)}\right) + 3.033\left(\frac{t(r)}{c(r)}\right); \quad (12)$$

where: $f(r)$ is the camber distribution, $c(r)$ is the chord distribution, $t(r)$ is the thickness distribution and $\sigma(r)$ is the local cavitation number. Solving for the chord distribution we have:

$$c(r) = \frac{|8.09f + 3.033t|}{2\sigma} + \frac{\sqrt{|8.09f + 3.033t|^2 + 4\sigma|26.67f^2 + 10ft|}}{2\sigma} \quad (13)$$

With linearized, ideal, two-dimensional camber we have:

$$f(r) = \frac{2\pi}{\kappa} DG(r)\frac{V_s}{V^*}; \quad (14)$$

where $\kappa = 15.035$ for this foil section.

For small cavitation numbers, $\sigma(r) < 0.54$, $c(r)$ from equation 13 is used as the minimum chord length. For intermediate cavitation numbers, $0.54 < \sigma(r) < 1.16$, the chord is further required to be greater than five times the local thickness as well as twenty times the camber. For larger cavitation numbers the restrictions on thickness and camber remain, but the chord length is no longer required to satisfy equation 13.

# 4 Duct Effects on the Propeller Flowfield

The presence of the duct will alter the flowfield of the lifting line and consequently the expressions for the thrust and the torque of the propeller.

To determine the effect of the duct on the lifting lines we first find the potential on the duct due to the lifting lines, and then determine the velocities on the lifting lines induced by that potential on the duct.

The loading on the propeller will be approximated by $M$ discrete constant strength horseshoes as described in the previous section. The geometry of the trailing vortices in the wake will be assumed frozen. A discussion of wake alignment can be found in section 7.

The potential $\phi_{LL}$ on the duct induced by the lifting lines can be decomposed as follows:

$$\phi_{LL} = \sum_{m=1}^{M} \Gamma_m \, \phi_{LL,m}; \quad (15)$$

where $\Gamma_m$ is the strength of the $m^{th}$ horseshoe and $\phi_{LL,m}$ is the potential on the duct induced by the $m^{th}$ unit strength horseshoe.

The potential $\phi_{LL,m}$ is determined by converting the discrete vortex loops which form the $m^{th}$ horseshoe into constant strength dipole panels, as shown in Figure 3 and then by computing the effect of each of those panels as descibed by Newman [13].

Equation 2 is linear with respect to $\phi_{LL}$. Therefore, the perturbation potential, $\phi_D$, on the duct can be expressed as:

$$\phi_D = \phi_{D,0} + \sum_{m=1}^{M} \Gamma_m \, \phi_{D,m}; \quad (16)$$

where $\phi_{D,m}$ is the potential on the duct due to the interaction of the duct with the $m^{th}$ unit strength horseshoe. It satisfies the equation:

$$2\pi\phi_{D,m} = \int\int_{S_D} \phi_{D,m}\frac{\partial}{\partial n}\frac{1}{R}dS + \int\int_{S_W} \Delta\phi_{D,m}\frac{\partial}{\partial m}\frac{1}{R}dS - 4\pi\phi_{LL,m}, \quad (17)$$

and $\phi_{D,0}$ is the potential on the duct due to the interaction of the duct with the incoming flow $\vec{U}_{in}$. It satisfies the equation:

$$2\pi\phi_{D,0} = \int\int_{S_D} [\phi_{D,0}\frac{\partial}{\partial n}\frac{1}{R} + [\vec{U}_{in}.\vec{n}]\frac{1}{R}]dS + \int\int_{S_W} \Delta\phi_{D,0}\frac{\partial}{\partial n}\frac{1}{R}dS. \quad (18)$$

The total velocity $\vec{q}$ at any point in the flowfield and with respect to the propeller rotating frame can then be expressed as:

$$\vec{q} = \vec{U}_{in} + \vec{q}_{LL} + \sum_{m=1}^{M} \Gamma_m \, \vec{q}_{D,m} + \vec{q}_{D,0}. \quad (19)$$

- $\vec{q}_{LL}$ is the velocity induced by the lifting lines and their trailing wakes.
- $\vec{q}_{D,m}$ is the velocity due to the interaction between the duct and the $m^{th}$ unit strength horseshoe. It is computed as the summation of the velocities induced by the dipoles on the duct and its wake of strengths $\phi_{D,m}$ and $\Delta\phi_{D,m}$, respectively.
- $\vec{q}_{D,0}$ is the velocity due to the interaction of the duct with the incoming flowfield $\vec{U}_{in}$. It is computed as the summation of the velocities induced by the sources on the duct of strength $-\vec{U}_{in}\cdot\vec{n}$ and the dipoles on the duct and its wake of strengths $\phi_{D,0}$ and $\Delta\phi_{D,0}$, respectively.

# 5 The Ducted Propeller Optimization Scheme

The variational circulation optimization procedure can be readily modified to account for the propeller-duct velocity interactions. This is done by simply modifying the inflow velocities to the lifting lines and the velocities induced by the unit circulation horseshoes. In other words the propeller optimization equations remain the same, only the inflow velocities and the "induction factors" in equation 11 are changed. The present theory does not take into account the effect of duct forces on the optimum distribution of circulation. This limitation is addressed in section 7.2.

The axial velocity at each control point due to the duct in the absence of the propeller's vortex system, $(V_{Am})_{\text{duct}}$, is added to the inflow velocity, $(V_{Am})_{\text{inflow}}$.

$$V_{Am} = (V_{Am})_{\text{inflow}} + (V_{Am})_{\text{duct}}; \quad m = 1, \ldots, M. \quad (20)$$

$(V_{Am})_{\text{duct}}$ is the axial component of the velocity $\vec{q}_{D,0}$ on the plane of the propeller at the radius of a control point $m$. An axisymmetric duct acting alone has no effect on the tangential velocity component, and the radial component of velocity does not enter into the computation of propeller forces.

Similarly, the velocities induced at each control point, $m$, by a horseshoe vortex of unit strength surrounding each control point, $n$, in the absence of a duct are added to similar velocities induced by the duct in the presence of such a vortex.

$$\begin{aligned} u^*_{m,n} &= (u^*_{m,n})_{\text{propeller}} + (u^*_{m,n})_{\text{duct}}; \\ v^*_{m,n} &= (v^*_{m,n})_{\text{propeller}} + (v^*_{m,n})_{\text{duct}}; \\ & m = 1, \ldots, M; \qquad n = 1, \ldots, M. \end{aligned} \quad (21)$$

The velocities $(u^*_{m,n})_{\text{duct}}$ and $(v^*_{m,n})_{\text{duct}}$ correspond to the axial and tangential components of the velocity $\vec{q}_{D,n}$ evaluated on the plane of the propeller at the radius of a control point $m$.

## 5.1 Panel Method Duct

The velocities in equations 20 and 21 induced by a given duct and propeller vortex wake geometry can be accurately computed using a panel method as previously described. Since the panel method computation is done with unit circulations on each horseshoe, this computation need only be run once for any given duct and propeller wake geometry. This computation is a relatively large one. However, many propeller thrusts or variations to the propeller optimization scheme may be tested using stored values from a single run of the panel method.

The use of a panel method also allows for an accurate computation of duct forces, if the potential on the duct induced by each of the unit horseshoe vortices is stored. An approximate value for the viscous drag on the duct can be subtracted from the duct thrust. This viscous drag is simply taken to be

$$D = \frac{1}{2} V_S^2 c\pi D (C_D)_{\text{duct}}; \quad (22)$$

where $c\pi D$ is the projected area of the duct.

## 5.2 Image Duct

If the duct geometry is greatly simplified to that of a cylindrical solid boundary of infinite chord and constant radius, $r_{\text{duct}}$, surrounding a propeller, then it is possible to approximately model a propeller operating inside a duct simply as the propeller's bound and trailing vortex system combined with a system of image trailing vortices of equal and opposite strength. The radius of each helical image vortex is given by

$$(r_n)_{\text{image}} = \frac{(r_n)^2_{\text{duct}}}{r_n}; \qquad n = 1, \ldots, N; \quad (23)$$

where $N = M+1$. The pitch of the image vortex system is given by

$$\tan(\beta_n)_{\text{image}} = \frac{r_n}{(r_n)_{\text{image}}} \tan\beta_n; \qquad n = 1, \ldots, N. \quad (24)$$

This system satisfies the boundary condition of zero normal velocity to the infinite duct correctly for helices of infinite pitch.

This image vortex system provides for no forces on the duct. However, the velocites induced by this system can be efficiently computed in the same manner as for the propeller's trailing vortex system. The usefullness of this image duct approach will be investigated in section 7.1.

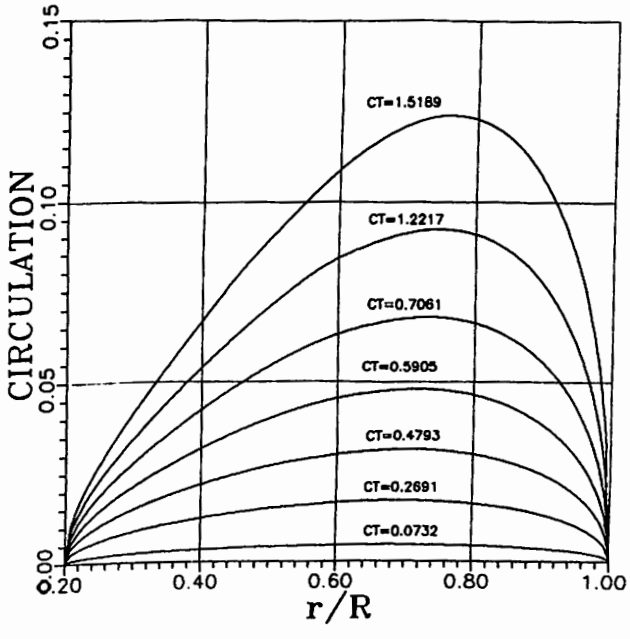


Figure 6: Optimum radial distribution of circulation for a free-running propeller. The nondimensional circulation is given by $G = \Gamma/(\pi D V_S)$. $J = V_S/(nD) = 1.143$. $C_T = 8T/(\rho\pi V_S^2 D^2)$ varies from 0.0732 to 1.5189.

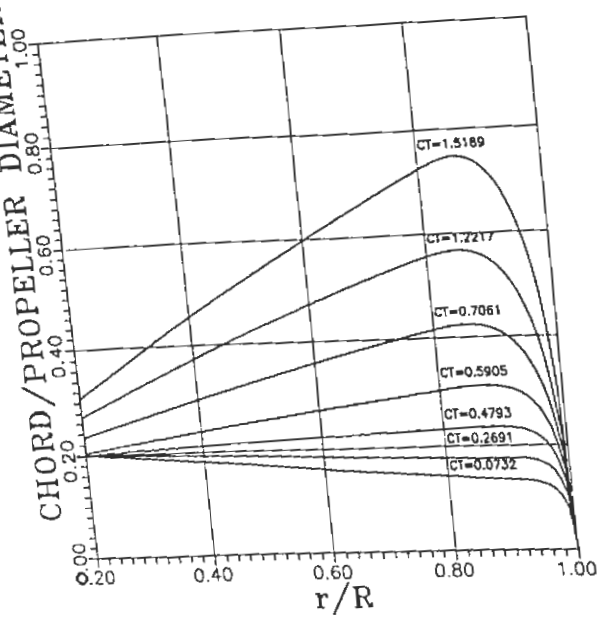


Figure 7: Chordlength distribution for a free-running propeller.
$J = V_S/(nD) = 1.143$. $C_T = 8T/(\rho\pi V_S^2 D^2)$ varies from 0.0732 to 1.5189.

## 6 Results

The present theory was used to determine optimum load distributions and chord lengths for a four bladed propeller operating inside of two duct geometries. The propeller was assumed to be hubless, with a root radius of twenty percent of the propeller radius. The root chord was required to be at least twenty percent of the propeller diameter. For simplicity, the blade thickness was everywhere assumed to be one percent of the propeller diameter, and the two-dimensional sectional drag coefficient was everywhere assumed to be 0.0085.

The variational optimization procedure was used to find optimum circulation distributions for a series of free-running, unducted propellers operating at a fixed advance coefficient, $J = V_S/(nD)$, of 1.143. The propellers were each required to generate a different thrust. The thrust coefficient, $C_T = 8T/(\rho\pi V_S^2 D^2)$, was varied between 0.0732 and 1.5189. Figure 6 gives the circulation distributions and figure 7 gives the radial distribution of chordlength. The circulation is nondimensionalized in the usual way, $G = \Gamma/(\pi D V_S)$. Note how the circulation falls off to zero at the hub and tip. These runs for a propeller operating alone each took less than a second of CPU time on a VAXstation II computer.

Two duct geometries were investigated. Both had section angles of attack of 10.2 degrees. The duct thicknesses and cambers were given by NSRDC modified NACA 66 thickness forms [2] and $a = 0.8$ mean lines with parabolic tails [1]. A two-dimensional sectional drag coefficient of 0.0085 was used. The two duct geometries are given in figure 8. In each case the propeller lifting lines were placed at an axial location 40 percent of the way between the leading and trailing edges of the duct.

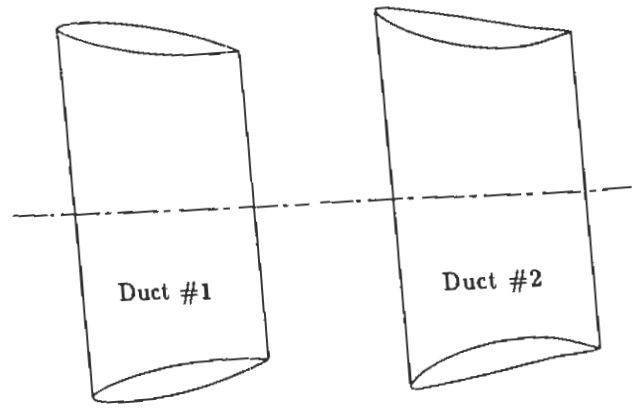


Figure 8: Duct geometries

**Duct #1** This duct is uncambered, with a section chordlength of 0.584 times the propeller diameter. This duct has a maximum thickness to chord ratio of 15 percent.

**Duct #2** This duct has a section chordlength of 0.632 times the propeller diameter. It also has a thickness to chord ratio of 15 percent, but this duct is cambered with a camber to chord of ratio 7 percent.

The total axial velocities inside of the two ducts operating in open water are shown in Figure 9. These velocities are computed at the propeller plane, but in the absence of a propeller. These are the axial components of the velocity, $\vec{q}_{D,0}$, added to the axial component of the incoming flowfield, $\vec{U}_{in}$, which for these free-running ducts is the ship's velocity, $V_S$. Note that the uncambered duct, Duct #1, decelerates the flow in

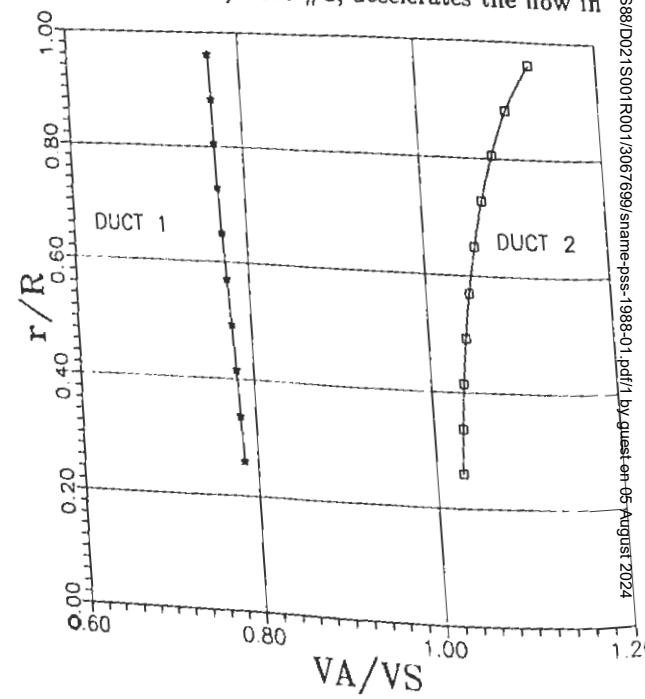


Figure 9: Total axial velocities, at the propeller plane, in the presence of a duct operating in open water, but in the absence of a propeller.

the absence of a propeller, while the cambered duct accelerates the inflow. We will finally show that both of these ducts can generate thrust under some conditions and thus would be known as "accelerating" ducts. It is the interaction of the duct and the propeller that results in a flow acceleration for "thrusting" ducts.

For all of the cases shown, the duct is represented by 80 chordwise panels and 120 circumferential panels. The propeller is represented by 10 horseshoe vortices. Approximately six hours of CPU time is taken on a VAXstation II to find the potentials and velocities due to the system of unit horseshoes interacting with the duct. Once these solutions have been obtained, it takes about 15 seconds of CPU to obtain an optimum circulation distribution and duct and propeller forces for each desired thrust coefficient.

Figures 10 and 11 give the radial distributions of circulation and chord for a propeller operating inside of Duct #1. The advance coefficient is the same as that of the unducted propeller examined earlier, $J = 1.143$. Note in Figure 10 that the circulation at the tip no longer falls off to zero. The presence of this tip loading implies that the propeller circulation is being transferred to the duct and is not being shed into the wake as a tip vortex.

Figure 12 plots the thrust coefficient of that portion of the thrust generated by the duct against the total thrust coefficient. Shown are results for both ducts operating at an advance coefficient of 1.143. Notice that for smaller total thrusts there is a net drag on the duct. At zero thrust, which corresponds to zero loading, this drag consists entirely of the viscous drag on the ducts. For small, but nonzero, loadings there is also some inviscid drag generated on the ducts. At higher total thrust there is thrust, not drag, generated by both ducts. For large thrust coefficients these ducts would thus be considered to be "accelerating" or "thrusting." For small loadings these ducts would be called "decelerating." The duct thrust appears to be quadratic with the total thrust. The inviscid part of the duct thrust is a quadratic function of the horseshoe circulations.

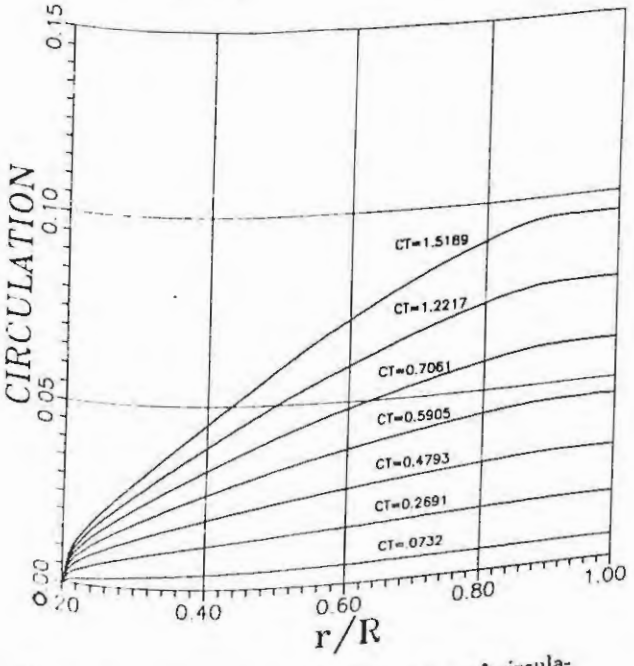


Figure 10: Optimum radial distribution of circulation for a propeller operating inside of Duct #1. $J = 1.143$. $C_T$ based on the total thrust varies from 0.0739 to 1.5321.

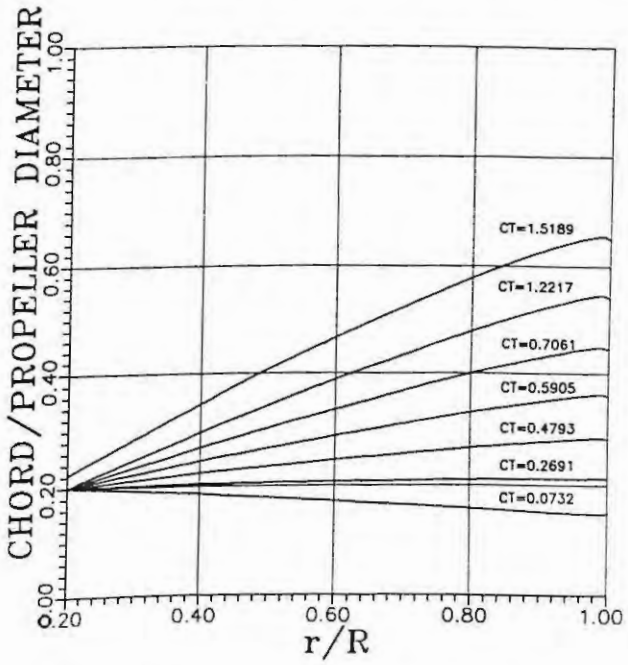


Figure 11: Radial distribution of chordlength for a propeller operating inside of Duct #1. $J = 1.143$. $C_T$ based on the total thrust varies from 0.0739 to 1.5321.

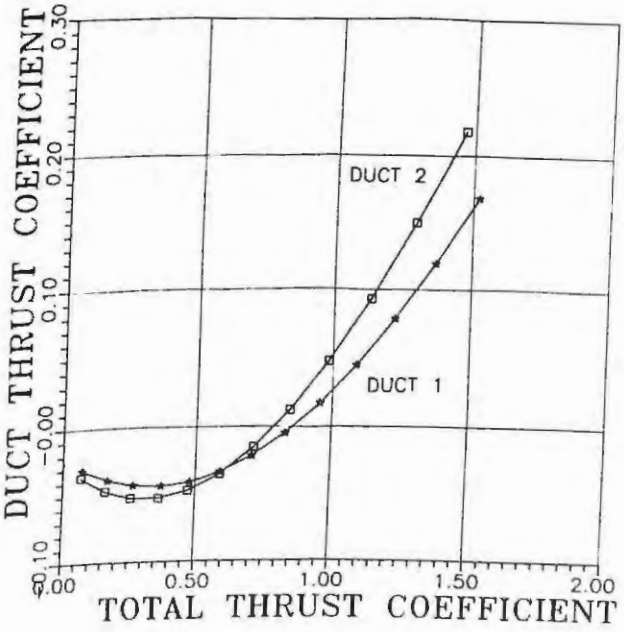


Figure 12: Duct thrust coefficient as a function of the total thrust coefficient. $J = 1.143$.

Figure 13 gives the fraction of the total thrust generated on the propeller as a function of the total thrust coefficient for both ducts at $J = 1.143$. Figure 14 is a plot of propulsive efficiency vs the thrust coefficient for "optimum" propellers operating inside the ducts as well as for the unducted propeller at this same advance coefficient. Note that for this operating condition the uncambered duct is generally more efficient than the unducted propeller which, is in turn, more efficient than the cambered duct. These trends will apparently be reversed at higher thrust coefficients.

Figures 16 through 18 give similar results for Duct #1 operated at three different advance coefficients, $J = 0.842$, $J = 1.143$ and $J = 1.814$. Figures showing the propeller expanded area ratios, duct thrust coefficients, fractions of the total thrust generated on the propeller and the propulsive efficiency, all as a function of total thrust coefficient, are given.

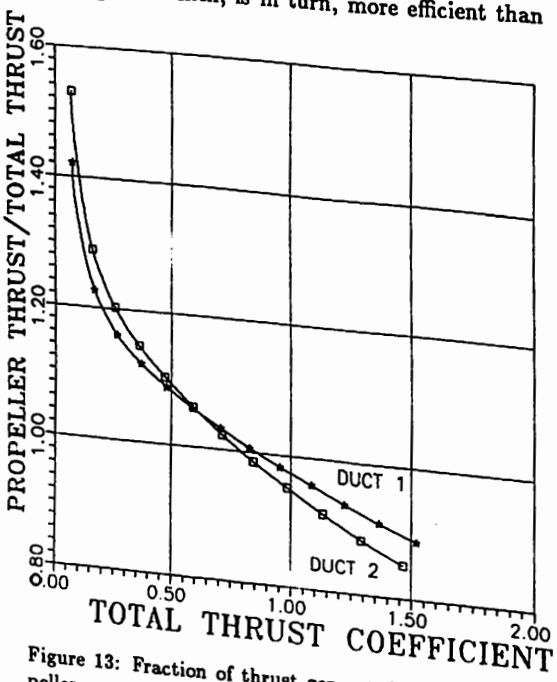


Figure 13: Fraction of thrust generated on the propeller as a function of the total thrust coefficient. $J = 1.143$.

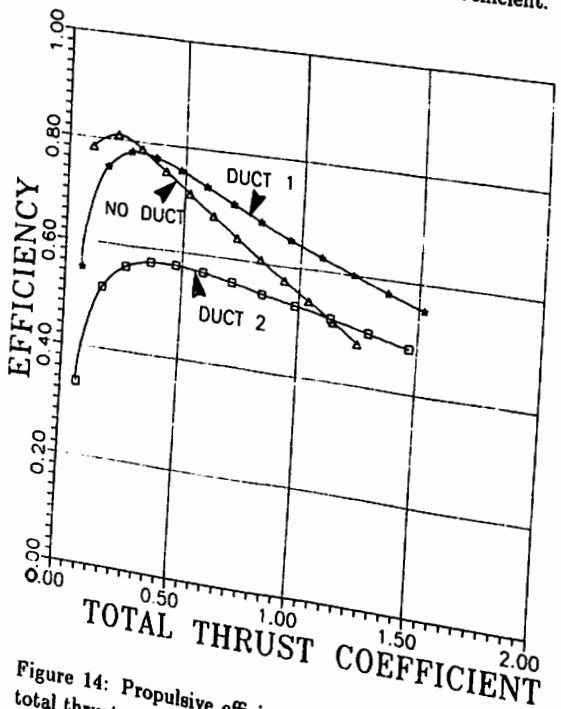


Figure 14: Propulsive efficiency, $\eta$, as a function of total thrust coefficient. $J = 1.143$.

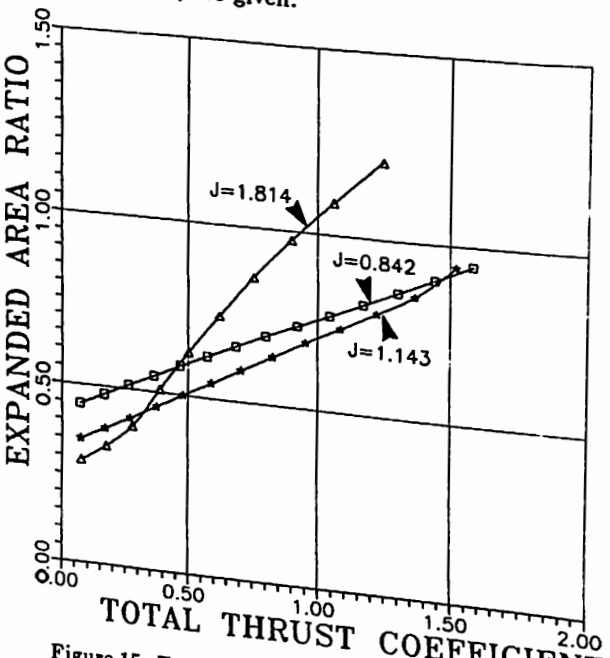


Figure 15: Expanded area ratio, $A_E/A_0$, as a function of total thrust coefficient. Duct #1.

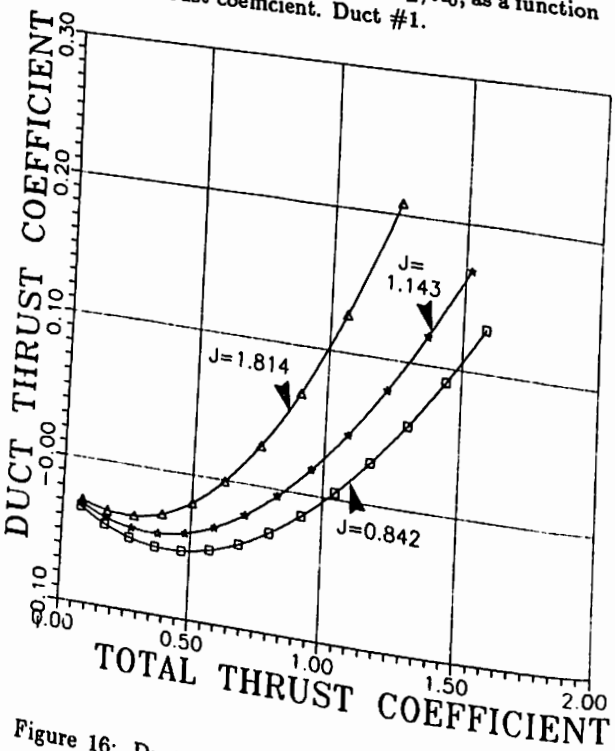


Figure 16: Duct thrust coefficient as a function of total thrust coefficient. Duct #1.

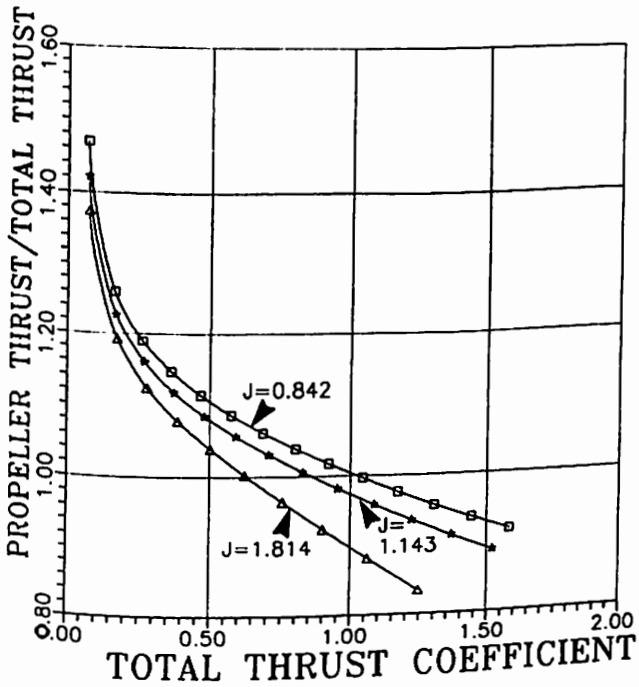


Figure 17: Fraction of total thrust generated on the propeller as as a function of total thrust coefficient. Duct #1.

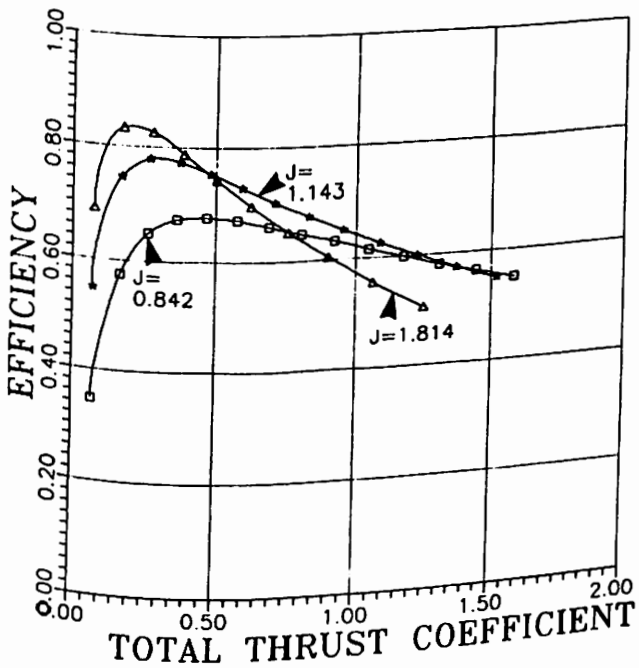


Figure 18: Propulsive efficiency, $\eta$, as a function of total thrust coefficient. Duct #1.

# 7 Future Considerations

As described, the current theory finds the optimum radial distribution of circulation on the propeller acting in the nonaxisymmetric velocity field of a given axisymmetric duct. The effect of thrust or drag generated by the duct on the circulation distribution is not included; i.e. the duct thrust is computed, but its value is not optimized.

Clearly, these results are useful, but limited. The authors feel that they have, as yet, only developed the framework for combining lifting line circulation optimization techniques with the velocity prediction abilities of panel methods. Following are descriptions of some of the extensions to these ideas that the authors intend to pursue.

## 7.1 Wake Adaption and Alignment

The current theory allows only for helical vortex wakes aligned with the propeller's rotation and a uniform inflow velocity. Moderately loaded, wake adapted, propeller lifting line theory calls for the still purely helical vortex wakes to be aligned with the induced flow at the lifting line. This is easily accomplished in the case of a propeller operating alone by iteratively modifying the pitch of each helix with the induced velocities.

In the case of a propeller operating inside a duct modelled by a panel method, the duct must be repanelled and the problem resolved with each iteration of the wake alignment procedure, if the change in the pitch of the helices is substantial. The authors feel that this procedure would be too expensive in computer time. Instead, they propose using a simple model for the ducted propeller, that of the propeller plus an image vortex system together with inflow velocities to the propeller from the duct operating in the absence of the propeller, to align the wake and estimate the circulation distribution. This wake would then be held frozen within a modified version of the current procedure. This procedure should work if the circulation predicted by the propeller and its image vortex system is close to the final value from the panel method. To see if this might be the case, a comparison of the circulation distribution predicted with duct induced velocities from the panel method and from an image duct was made. The results are shown in figure 19.

In this example the operating condition was chosen so that the wake was "automatically" aligned. That is, the velocity field created by the duct in the absence of the propeller added to the velocities induced by the propeller-duct system resulted in a helical wake which would be left approximately unchanged by wake alignment.

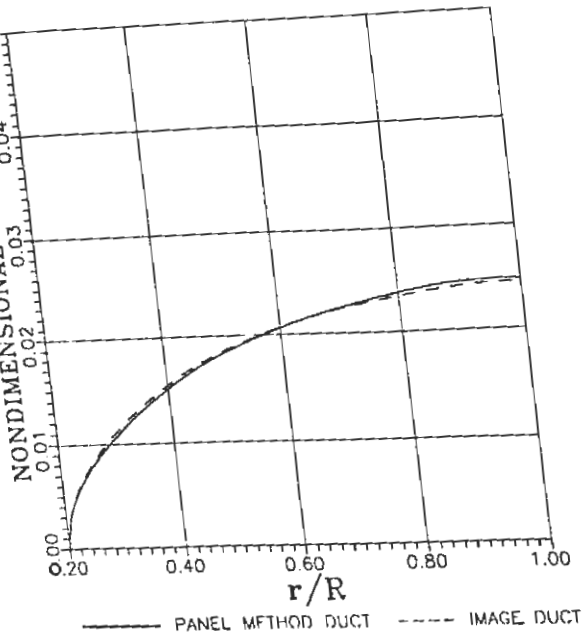


Figure 19: A comparison of the radial distribution of circulation predicted by the optimization procedure with duct induced velocities from a panel method and by an image vortex system. Duct #1. $J = 1.143$. $C_T = 0.45$.

### 7.2 Effect of Duct Forces on Propeller Circulation

The current theory finds the optimum radial distribution of circulation on the propeller acting in the velocity field of a given duct under the frozen wake assumption. The thrust or drag generated by the duct is computed, but its effect on the optimum circulation distribution is not included. It is possible to write out the thrust on the duct as a function of the circulation on each of the propeller's vortex horseshoes. The variational optimization equations could then be rewritten with the effect of duct thrust on propeller circulation included.

### 7.3 "Optimum" Duct Geometry

On a more speculative note, it would be desirable to input some global propeller-duct characteristic, typically the distribution of thrust between the propeller and the duct, and get back both the circulation on the propeller and the duct geometry. An investigation of how various duct parameters, such as angle of attack, camber, etc., interact with the optimum propeller might lead to a simple scheme to determine such an optimum duct geometry.

### 7.4 Non-axisymmetric Ducts

The potential based panel method for the analysis of axisymmetric ducts, as briefly described in section 2 of this paper and in some detail by Kerwin, Kinnas, et al. [9], has been extended in order to treat nonaxisymmetric ducts. A description of this extension and a comparison with experimental results is given by Nicholson [14].

## 8 Conclusions

A vortex lattice lifting line representation of a propeller has been combined with a panel method representation of a duct. This hybrid scheme allows for the accurate panel method computation of the nonaxisymmetric velocities induced by the duct, combined with the force prediction ability of a lifting line approach. Lifting line optimization techniques can then be applied to find optimum propeller load distributions.

While this technique is still in its formative stage, the authors feel that it will eventually evolve into a method for the detailed design of ducted propellers. The variational optimization technique is of special interest because it can readily be extended to address the optimum load distributions of multiple stage propulsors as decribed by Kerwin, Coney and Hsin [8]. Multiple stage ducted propulsors are of particular importance since stages of stator blades can be used to support the duct.

## Acknowledgements

Support for this project was in part provided by the MIT SeaGrant College Program grant number NA86AA-D-SG089, project R-T-24, Hydrodynamics of Marine Propulsors.

The authors wish to thank Professor Justin E. Kerwin for his valuable comments and suggestions in the development of this work.

# References


[1] I.H. Abbott and A.E. Von Doenhoff. *Theory of Wing Sections.* Dover, New York, 1959.

[2] T. Brockett. *Minimum Pressure Envelopes for Modified NACA-66 Sections with NACA a=0.8 Camber and Buships Type I and Type II Sections.* Report 1780, DTNSRDC, Teddington, England, Feb 1966.

[3] E.B. Caster. *A Computer Program for Use in Designing Ducted Propellers.* Technical Report 2507, NSRDC, 1967.

[4] J.A.C. Falcão de Campos. *On the Calculation of Ducted Propeller Performance in Axisymmetric Flows.* Technical Report 696, Netherlands Ship Model Basin, Wageningen, The Netherlands, 1983.

[5] Jinzhang Feng and Shitang Dong. *A Method for the Prediction of Unsteady Hydrodynamic Performance of the Ducted Propeller With a Finite Number of Blades.* Technical Report 85006, China Ship Scientific Research Center, Wuxi,China, August 1985.

[6] Dyne G. *A Method for the Design of Ducted Propellers in a Uniform Flow.* Technical Report 62, Swedish State Shipbuilding Tank, Goteberg, Sweden, 1967.

[7] I.S. Gibson and R.I. Lewis. Ducted propeller analysis by surface vorticity and actuator disc theory. In *Proceedings of the Symposium on Ducted Propellers*, The Royal Institution of Naval Architects, Teddington, England, MAY 1973.

[8] J.E. Kerwin, W.B. Coney, and C-Y. Hsin. Optimum circulation distributions for single and multicomponent propulsors. In *American Towing Tank Conference*, 1986.

[9] J.E. Kerwin, S.A. Kinnas, J-T. Lee, and W-Z. Shih. A surface panel method for the hydrodynamic analysis of ducted propellers. *Trans. SNAME*, vol 95, 1987.

[10] N.B. Kroeger. *Optimizatin of Propulsion Speeds.* Master's thesis, Department of Ocean Engineering, MIT, June 1972.

[11] W.B. Morgan. Theory of the annular airfoil and ducted propeller. In *Fourth Symposium on Naval Hydrodynamics*, pages pp 151-197, 1962.

[12] L. Morino and C-C. Kuo. Subsonic potential aerodynamic for complex configurations : a general theory. *AIAA J.*, vol 12(no 2):pp 191–197, February 1974.

[13] J.N. Newman. Distributions of sources and normal dipoles over a quadrilateral panel. *Journal of Engineering Mathematics*, vol 20:pp 113–126, 1986.

[14] S.J. Nicholson. *Propeller Onset Flow Alterations due to a Nonazisymmetric Duct.* Master's thesis, Department of Ocean Engineering, MIT, October 1987.

[15] Van Houten R. *Analysis of Ducted Propellers in Steady Flow.* Technical Report 4.76-1, Airflow Research and Manufacturing Corp., Watertown, MA., February 1986.

[16] D.F. Rogers and J.A. Adams. *Mathematical Elements for Computer Graphics.* McGraw-Hill, 1976.

[17] P.G. Ryan and E. Glover. A ducted propeller design method: a new approach using surface vorticity distribution techniques and lifting line theory. *Trans.*, vol 114, 1972.

[18] J.A. Sparenberg. On optimum propellers with a duct of finite length. *Journal of Ship Research*, vol 13(no 2), 1969.

[19] J.A. Sparenberg. On optimum propellers with a duct of finite length II. *Journal of Ship Research*, vol 14(no 4), 1970.

[20] J.W. Wrench. *The Calculation of Propeller Induction Factors.* Technical Report 1116, DTMB, 1957.